Does Perthionitrite (SSNO −) Account for Sustained Bioactivity of NO? A (Bio)chemical Characterization

ARTICLE *in* INORGANIC CHEMISTRY · JUNE 2015

Impact Factor: 4.76 · DOI: 10.1021/acs.inorgchem.5b00831

CITATION
1

READS
82

9 AUTHORS, INCLUDING:

Tatyana Shubina
Friedrich-Alexander-University of Erlangen-Nü…
83 PUBLICATIONS **1,299** CITATIONS
SEE PROFILE

Frank W. Heinemann
Friedrich-Alexander-University of Erlangen-Nü…
498 PUBLICATIONS **6,099** CITATIONS
SEE PROFILE

Ivana Ivanović-Burmazović
Friedrich-Alexander-University of Erlangen-Nü…
120 PUBLICATIONS **1,453** CITATIONS
SEE PROFILE

Milos Filipovic
University of Bordeaux
47 PUBLICATIONS **664** CITATIONS
SEE PROFILE

Inorganic Chemistry

Forum Article

pubs.acs.org/IC

Does Perthionitrite ($SSNO^-$) Account for Sustained Bioactivity of NO? A (Bio)chemical Characterization

Rudolf Wedmann,[†] Achim Zahl,[†] Tatyana E. Shubina,[†] Maximilian Dürr,[†] Frank W. Heinemann,[†] Bernhard Eberhard Christian Bugenhagen,[‡] Peter Burger,[‡] Ivana Ivanovic-Burmazovic,*[,†] and Milos R. Filipovic*[,†]

[†]Department of Chemistry and Pharmacy, Friedrich-Alexander University of Erlangen-Nuremberg, Egerlandstrasse 1, 91058 Erlangen, Germany

[‡]Department of Chemistry, University of Hamburg, Martin-Luther-King-Platz 6, 20146 Hamburg, Germany

Supporting Information

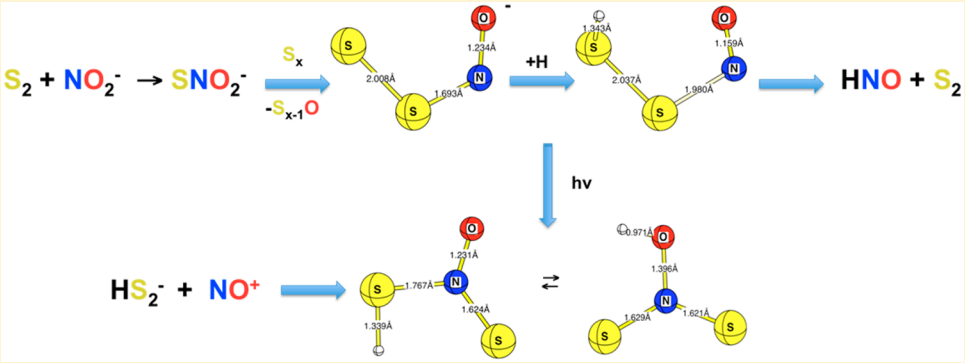

ABSTRACT: Hydrogen sulfide (H_2S) and nitric oxide (NO) are important signaling molecules that regulate several physiological functions. Understanding the chemistry behind their interplay is important for explaining these functions. The reaction of H_2S with *S*-nitrosothiols to form the smallest *S*-nitrosothiol, thionitrous acid (HSNO), is one example of physiologically relevant cross-talk between H_2S and nitrogen species. Perthionitrite ($SSNO^-$) has recently been considered as an important biological source of NO that is far more stable and longer living than HSNO. In order to experimentally address this issue here, we prepared $SSNO^-$ by two different approaches, which lead to two distinct species: $SSNO^-$ and dithionitric acid [HON(S)S/HSN(O)S]. (H)S_2NO species and their reactivity were studied by ^{15}N NMR, IR, electron paramagnetic resonance and high-resolution electrospray ionization time-of-flight mass spectrometry, as well as by X-ray structure analysis and cyclic voltammetry. The obtained results pointed toward the inherent instability of $SSNO^-$ in water solutions. $SSNO^-$ decomposed readily in the presence of light, water, or acid, with concomitant formation of elemental sulfur and HNO. Furthermore, $SSNO^-$ reacted with H_2S to generate HSNO. Computational studies on (H)SSNO provided additional explanations for its instability. Thus, on the basis of our data, it seems to be less probable that $SSNO^-$ can serve as a signaling molecule and biological source of NO. $SSNO^-$ salts could, however, be used as fast generators of HNO in water solutions.

INTRODUCTION

Gasotransmitter cross-talk is emerging as an important field of research that can provide mechanistic background to the physiological effects usually assigned to only one of them. Both nitric oxide (NO) and hydrogen sulfide (H_2S) are involved in the regulation of several important physiological processes such as the regulation of blood pressure,[1,2] neurotransmission,[3,4] immune defense,[5,6] etc. Others[7−10] and we[11−17] have shown that H_2S could react with NO[11] and its metabolites, such as peroxynitrite,[12,13] nitrite,[14,15] and *S*-nitrosothiols.[16,17]

The reaction between H_2S and *S*-nitrosothiols was of particular interest because it deals with a post-translational modification of proteins (S-nitrosation)[18−20] and could explain how S-nitrosation could be regulated in the cells. We characterized thionitrous acid (HSNO),[16] the smallest *S*-nitrosothiol, as a product of this reaction. HSNO was shown to have a short half-life, but it could still cross the biological membranes and control intra- or intercompartmental S-nitrosation.[16] Furthermore, HSNO could serve as both a source of NO and its redox congener, nitroxyl (HNO). As an additional product of this reaction, we observed a yellow compound, which showed neither a ^{15}N NMR signal nor a IR spectrum characteristic for NO vibration.[16] This relatively stable compound precipitates in time to give elemental sulfur.

Special Issue: Small Molecule Activation: From Biological Principles to Energy Applications

Received: April 12, 2015

DOI: 10.1021/acs.inorgchem.5b00831
Inorg. Chem. XXXX, XXX, XXX−XXX

On the basis of all of this, we proposed that this is a mixture of polysulfides.

It has recently been proposed that this stable product is, in fact, another *S*-nitrosothiol, namely, perthionitrite ($SSNO^-$).[21−23] The reevaluation of the reaction between *S*-nitrosothiols and H_2S performed in these studies led to the same biological effects[22] as those reported previously by us.[16] However, the observed effects were ascribed to the formation of $SSNO^-$ as a putative, stable species and slow-releasing donor of NO and/or HNO.[21−23] However, these studies did not provide chemical characterization of $SSNO^-$ under the corresponding experimental conditions.

The formation of $SSNO^-$ was originally achieved under strict aprotic and anaerobic conditions in the form of its bis(triphenyl)phosphaniminium (PNP) salt.[24] On the other hand, in the studies mentioned above,[21−23] the proposed mechanism for its formation in the biological milieu, starting from *S*-nitrosothiols, was based on the following reaction steps:

$$RSNO + H_2S \rightarrow HSNO + RSH \quad (1)$$

$$HSNO + H_2S \rightarrow HS_2^- + H^+ + HNO \quad (2)$$

$$HS_2^- + RSNO \rightarrow SSNO^- + RSH \quad (3)$$

In order to shed more light on the $SSNO^-$/HSSNO chemistry, we attempted to prepare it in situ in a reaction between H_2S_2 and NO^+, related to the proposed eq 3, as well as preparing its PNP^+SSNO^- salt and subsequently characterizing its biochemical reactivity. Our data unambiguously show that, although $SSNO^-$ could be prepared in dry organic solvents, $SSNO^-$ decomposes as soon as it gets into contact with water to give sulfur and HNO. This limits the possibility that $SSNO^-$ can act as a distinct biological signaling molecule.

EXPERIMENTAL SECTION

Chemicals. All chemicals were obtained from Sigma-Aldrich if not stated otherwise. All aqueous solutions were prepared using nanopure water. All buffers were supplemented with Chelex-100 resin and kept over the resin to remove traces of transition-metal ions. Organic solvents were purchased dry, additionally dried with $MgSO_4$, and stored in an argon box.

Disulfane Preparation. Hydrogen disulfide (H_2S_2) was synthesized according to a slightly modified literature protocol.[25] Namely, in a first step, crude sulfane ($Na_2S_{5.5}$) was generated by the reaction of elemental sulfur with $Na_2S{\cdot}9H_2O$. Excess sulfur and other impurities were removed by vacuum filtration. The resulting raw sulfane was subsequently added slowly to a solution of ice-cold concentrated hydrochloric acid (HCl) to facilitate another purification step. The purified raw sulfane was a yellow oil, which was separated from the aqueous phase in a separatory funnel. The raw sulfane was dried with P_2O_5 overnight. The yield was 80% (literature: 87%)[25] relative to the starting sulfur. To afford pure disulfane, a vacuum distillation of purified raw sulfane was performed, in which H_2S_3 (as a side product) and H_2S_2 were collected in Schlenk tubes at room temperature and at −80 °C, respectively. A total of 10 mL (literature: 15 mL)[25] of transparent-to-yellowish, liquid H_2S_2 was frozen, and then chloroform was added to dilute the mixture to a concentration of about 20 M (*and to stabilize the substance, which was prone to evaporation upon the slightest increase in temperature and to explosion if it came into contact with air/humidity*). This stock of H_2S_2 in $CHCl_3$ was stored under an argon atmosphere at −80 °C for not more than 2 weeks. New H_2S_2 was synthesized when needed. For experiments, the refrigerated stock of H_2S_2 was taken out and aliquots of diluted solutions in chloroform (about 600 mM) were made.

Synthesis of $^{15}NOBF_4$. ^{15}N-enriched $NOBF_4$ was synthesized from ^{15}N-enriched $NaNO_2$ according to the method by Connelly et al.[26] Specifically, to a mixture of water (250 μL), sulfuric acid (350 μL), and *n*-pentanol (1.5 mL, cooled to −10 °C) was slowly added a $Na^{15}NO_2$ solution (0.96 g in 4 mL). After 90 min of stirring, the reaction mixture was decanted from precipitated Na_2SO_4. The yellow layer of crude amyl nitrite was separated and dried over anhydrous $MgSO_4$ for 90 min. Over the course of 20 min, this crude amyl nitrite was added to a stirred mixture of 40% aqueous HBF_4 (3 mL) and propionic anhydride (18 mL, −15 °C). After 10 min of stirring at −15 °C, the white precipitate of $^{15}NOBF_4$ was filtered off, washed with propionic anhydride at −15 °C, and dried in a vacuum at room temperature overnight. The yield was 37%.

Preparation of Bis(triphenylphosphine)iminium Nitrite ($PNP^+NO_2^-$). $PNP^+NO_2^-$ was prepared from the respective chloride salt by salt metathesis using a literature protocol, slightly modified.[27] Specifically, 2 g of PNP^+Cl^- (3.484 mmol) were dissolved in 25 mL of warm water (80 °C) to achieve a saturated solution. After the salt dissolved completely, a nearly saturated solution of $NaNO_2$ (10 g in 13 mL; 0.145 mol) in water preheated to 80 °C was added to the former solution in the course of 1 h. Precipitation started right from the beginning of the addition. The solution was set aside on room temperature for 30 min and subsequently stored on ice for another 1.5 h. The solution was filtered, and a slimy white precipitate was obtained. This was dissolved in 15 mL of anhydrous acetonitrile, to which $MgSO_4$ was added to further dry the reaction mixture. The solution was stirred for 2 h, and $MgSO_4$ was separated by filtration. Acetonitrile was removed by distillation, and the (white to slightly orange) residuum was dissolved in 12 mL of dry acetone (which, in turn, became slightly orange). The solution was filtered through a 0.45 μm poly(tetrafluoroethylene) (PTFE) filter, yielding a completely clear filtrate. A total of 7 mL of dry diethyl ether was added to initiate crystallization. The flask was stored at −28 °C overnight. The next day, the crystallized fraction was filtered and dried (1.52 g, 2.6 mmol; 75% yield with respect to PNP^+Cl^-). For the preparation of ^{15}N-enriched $PNP^+NO_2^-$ from PNP^+Cl^-, an analogous procedure was used, starting out from ^{15}N-enriched $NaNO_2$ (77% yield with respect to PNP^+Cl^-).

Preparation of PNP^+SSNO^-. In a subsequent step, following a modified literature protocol,[24] 0.525 g of $PNP^+NO_2^-$ (900 μmol) and 57 mg of elemental sulfur (1.8 mmol as referred to "S") were weighed in a vial in the argon box, and 15 mL of dry acetone was added. The reaction mixture was stirred overnight, in the argon box, yielding a dark orange-to-red solution. This solution was PTFE-filtered to remove remnants of unreacted sulfur. To the reaction mixture was added 10 mL of dried diethyl ether to initiate crystallization. The majority of the crystals were red, with some trace amounts of yellow crystals. Crystals were dissolved in acetone and recrystallized by the addition of diethyl ether at least twice.

Absorption Spectroscopy. UV−vis measurements were performed in anaerobic cuvettes (i.e., cuvettes sealable with a screw cap equipped with a silicon/PTFE septum) using an HP 8452A diode-array spectrophotometer connected to a computer equipped with *Olis Spectralworks* software. Additional measurements were performed on a Specord 200 spectrophotometer by Jena Analytics, connected to a computer equipped with *Winaspect* software.

Fluorescence Measurements. Fluorescence measurements were recorded on a FP-8200 spectrofluorometer (Jasco, Gross-Umstadt, Germany) using anaerobic cuvettes. Fluorescence probes used in an aqueous medium were CuBOT1 (synthesized according to the published procedure; excitation 495 nm; emission 528 nm)[28] and 4-amino-5-(methylamino)-2′,7′-difluorofluorescein (DAF-FM; excitation 500 nm; emission 515 nm). A fluorescence probe used in acetone was dihydrorhodamine (DHR; excitation 500 nm; emission 530 nm).

X-ray Crystallography. Single crystals of the title compound suitable for X-ray diffraction were obtained by crystallization from acetone by the addition of diethyl ether. Red crystals were measured on a Bruker APEX2 diffractometer with Mo Kα radiation. Structure solution and least-squares refinement were performed with the software packages *SHELX*[29] and *OLEX2*.[30] The compound crystallizes in the orthorhombic space group *Pbcn* with four formula units in the

DOI: 10.1021/acs.inorgchem.5b00831
Inorg. Chem. XXXX, XXX, XXX−XXX

unit cell. The PNP^+ cation is situated on a crystallographic 2-fold rotation axis, as is the $SSNO^-$ anion, resulting in an asymmetric unit that contains half of a formula unit. Because of its situation on a 2-fold axis but missing molecular rotation symmetry, the $SSNO^-$ anion is disordered. A model consisting of two orientations of the anion with fixed occupation numbers of 0.5 has successfully been applied to treat the disorder so that reasonably precise geometrical data for the molecule could be extracted. CCDC 1058897 for PNP^+SSNO^- contains the supplementary crystallographic data. These data can be obtained free of charge from The Cambridge Crystallographic Data Centre via www.ccdc.cam.ac.uk/data_request/cif. A summary of important crystallographic data, data collection, and refinement details is presented in Table S1 in the Supporting Information (SI). Yellow crystals (CCDC 1058885), present in a trace amount, were also investigated on a SuperNova dual diffractometer using Cu Kα radiation and an AtlasS2 detector (see the SI, Table S1).

NMR Spectroscopy. ^{14}N and ^{15}N NMR spectra were recorded on a Bruker AVANCE DRX 400WB spectrometer equipped with a Spectrospin superconducting wide-bore magnet operating at a resonance frequency of 28.90 and 40.54 MHz, respectively, at a magnetic induction of 9.4 T. The measurements were performed with a commercial 5 mm Bruker broad-band probe thermostated with a Bruker B-VT 3000 variable-temperature unit. Chemical shifts given were referenced to nitromethane.

Electron Spin Resonance (ESR) Spectra. ESR spectra were collected at 90 K using a JEOL FA-200 ESR spectrometer. For scavenging of HNO and NO in an aqueous medium, diethyldithiocarbamate (DETC) complexes of Fe^{2+} and Fe^{3+} were used. Iron(III) *meso*-tetraphenylporphyrinato chloride was used to trap HNO in aprotic solvents.[31,32]

Cyclic Voltammetry. Cyclic voltammogramms were recorded at a PGSTAT 101 potentiostat (Metrohm, Filderstadt, Germany) in acetone using a platinum working electrode, a platinum counter electrode, and a Ag/AgCl reference electrode (2 M LiCl in EtOH, Metrohm, Filderstadt, Germany). A ferrocene solution was measured in the same setup as an additional reference. Tetrabutylammonium hexafluorophosphate (100 mM) was used as an electrolyte after extensive drying of the salt. The concentration of PNP^+SSNO^- in the experiment was 2 mM. The scan rates used ranged from 0.1 to 1.0 V/s. The voltammograms shown are referenced against a standard hydrogen electrode (SHE).

In Situ Fourier Transform Infrared (FTIR) Spectroscopy. In situ FTIR measurements in solutions were performed at a 45m React IR instrument (Mettler Toledo, Greifensee, Switzerland). Reactions monitored were those induced by the addition of $NOBF_4$ (the ^{14}N- and ^{15}N-enriched isotopic form) to H_2S_2 in chloroform, as well as by the addition of elemental sulfur to $PNP^+NO_2^-$ (the ^{14}N- and ^{15}N-enriched isotopic form) in acetone to initiate PNP^+SSNO^- formation.

FTIR Spectroscopy. FTIR measurements in a KBr matrix were performed on a Varian Excalibur FTS 3500GX FTIR spectrometer connected to a computer equipped with *Resolutions 4.0* software.

Electrospray Ionization Mass Spectrometry (ESI-MS). MS measurements were performed on a UHR-ToF Bruker Daltonik (Bremen, Germany) maXis, which was coupled to a Bruker cryospray unit. Detection was in positive and negative ion modes. The flow rates were 200 μL/h. The dry-gas (N_2) temperature was held at −20 °C, and the spray-gas temperature was held at −15 °C. The instrument was calibrated prior to every experiment via the direct infusion of an Agilent ESI-TOF (time-of-flight) low-concentration tuning mixture, which provided an m/z range of singly charged peaks up to 2700 Da in both ion modes. H_2S_2 and $NOBF_4$ were premixed (1:1 from a 600 mM stock of H_2S_2 in chloroform and a 600 mM stock of $NOBF_4$ in acetonitrile) immediately before injection into the instrument.

Cell Culture. The bovine arterial endothelial cell (BAEC) was used for cell-based experiments (CLS Cell Lines Service GmbH, Eppelheim, Germany). Cells were grown at 5% CO_2 in the recommended medium, Ham's F-12. The medium contained 10% fetal calf serum and a 1% penicillin/streptomycin solution. Cells were treated with acetonitrile solutions of 6 mM NO^+ (from a 600 mM $NOBF_4$ stock in CH_3CN), 6 mM H_2S_2 (from a 600 mM stock in $CHCl_3$), or a combination of both premixed in a separate tube immediately before the addition to the cell flask. After 1 h of treatment, cells were lysed by the addition of 0.1 mM HCl and the lysates used in the enzyme-linked immunosorbent assay (ELISA) (in triplicates). A set of standards were measured (for an eight-point calibration) together with the actual samples.

Detection of Protein S-Suflhydration and S-Nitrosation. $SSNO^-$-treated solutions of glyceraldehyde 3-phosphate dehydrogenase (GAPDH) and bovine serum albumin (BSA) were analyzed for oxidative modifications of cysteines. The protein concentrations were 1 mg/mL for GAPDH and 2.66 mg/mL for BSA. The PNP^+SSNO^- concentration used for protein treatment was 24 mM. Detection of S-nitrosylated BSA and GAPDH was performed using a modified biotin-switch assay.[33] Detection of S-sulfhydrated BSA and GAPDH was performed using a tag-switch assay modified from Zhang et al.[34]

Cyclic Adenosine Monophosphate (cAMP) Cyclic Guanosine Monophosphate (cGMP) Measurements. Quantification of cAMP and cGMP was performed using an indirect, competitive ELISA by Cayman Chemical, USA (Ann Arbor, MI). Post-treatment cell lysates of BAEC were used for two individual ELISAs (for cGMP and cAMP quantification, respectively), applying the procedure recommended by the manufacturer.

Computational Details. All structures were fully optimized at the SCS-MP3/aug-cc-pVTZ level of theory in combination with the corresponding Coulomb fitting basis for the resolution of identity.[35−38] The nature of the stationary points (minima or transition state) was characterized by calculations of frequencies numerically. Additionally, full optimization of key structures was performed with the aug-cc-pVQZ basis set, followed by single-point calculations at the CCSD(T)-F12*/cc-pVQZ-F12 (the auxiliary basis sets and complementary auxiliary basis sets developed for use with this basis set) level.[39−42] All MP3 calculations were performed with Orca 3.0.2 and CCSD(T)-F12*, with *Turbomole 6.6* programs.[43,44]

It is known that the description of the S−N bond length is drastically dependent on the chosen method. *cis*/*trans*-$SSNO^-$ was no different. However, with the availability of the crystal structure, we were able to choose a quite satisfactory method to describe $SSNO^-$ isomers. Geometries obtained at the spin-component-scaled MP3 level with the aug-cc-pVTZ basis set are in very good agreement with the X-ray data. An additional increase of the basis set leads to convergence of the relative energies.

RESULTS AND DISCUSSION

Product of the Reaction between H_2S_2 and NO^+. In the recent literature,[21,23] it has been suggested that $SSNO^-$ can be produced in the reaction of *S*-nitrosothiols with sulfide, which proceeds through the intermediate formation of HSNO (eq 1), its subsequent reaction with H_2S to form hydrogen persulfide (H_2S_2, eq 2), and the final interaction between H_2S_2 and an additional molecule of *S*-nitrosothiol (eq 3). This last step formally represents the metathesis of a proton in H_2S_2/HS_2^- by the nitrosonium cation (NO^+) of *S*-nitrosothiol, which leads to the formation of $SSNO^-$ (eq 3). Therefore, we wanted to probe this crucial reaction step in a direct manner by testing the reaction between H_2S_2 and $NO^+BF_4^-$, as a potential pathway for $SSNO^-$ generation.

Though a synthetic protocol for the preparation of H_2S_2 is known in the literature,[25] its synthesis remains challenging. H_2S_2 is a colorless to very pale-yellow liquid of pungent smell, different from that of other sulfide species. *H_2S_2 is highly unstable so that any trace of air and/or humidity led to explosion followed by the production of H_2S gas and elemental sulfur.* To stabilize the liquid H_2S_2, immediately after distillation under vacuum, it was frozen in liquid nitrogen and then diluted with dry chloroform. The solution prepared in this way was stable for several weeks when kept under argon and at −80 °C. The chloroform solution of H_2S_2 has an ^1H NMR chemical shift at

DOI: 10.1021/acs.inorgchem.5b00831
Inorg. Chem. XXXX, XXX, XXX−XXX

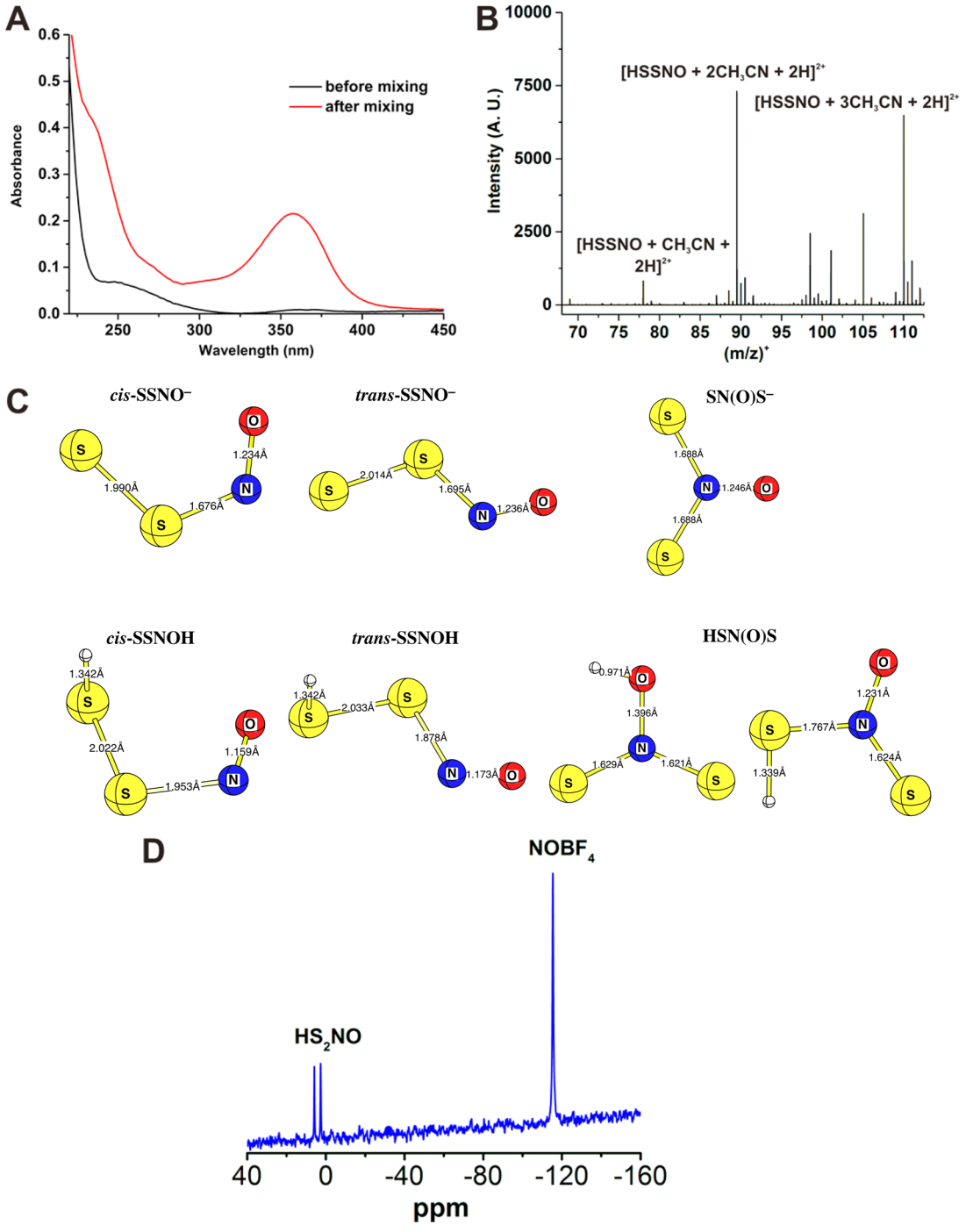

Figure 1. Reaction of H_2S_2 and $NOBF_4$ to form an HS_2NO isomer. (A) UV−vis spectral changes before (black line) and after (red line) the mixing of 60 mM acetonitrile solutions of H_2S_2 (from the stock in $CHCl_3$) and $NOBF_4$ in the tandem cuvette. (B) MS spectrum of the H_2S_2 + $NOBF_4$ reaction mixture obtained by positive-ion-mode cryo-ESI-TOF-MS. The acetonitrile/chloroform mixure (1:1, v/v) was sprayed at −40 °C. The capillary voltage was set to 4300 V, the collision energy to 8.0 eV, and the transfer time to 60 μs. The peaks observed at m/z 68.9976, 89.5088, and 110.0221 correspond to $[HS_2NO + CH_3CN + 2H]^{2+}$, $[HS_2NO + 2CH_3CN + 2H]^{2+}$, and $[HS_2NO + 3CH_3CN + 2H]^{2+}$, respectively. (C) Optimized geometries of the thermodynamically most stable isomers of S_2NO^- and their corresponding protonated forms, SCS-MP3/aug-cc-pVQZ. Bond lengths are in angstroms. (For further information, see Tables S2 and S3 in the SI, and for SCS-MP3/aug-cc-pVTZ-optimized geometries, see Figure S3 in the SI.) (D) ^{15}N NMR spectrum of the reaction mixture containing 60 mM H_2S_2 and 60 mM $^{15}NOBF_4$ in acetonitrile. The measurement was performed at −30 °C using a total number of 3072 scans with a relaxation delay of 5 s and a total recording time of 4 h 59 min. A 30° pulse was used.

2.0 ppm and a vibration band at 909 cm^{-1} (Figure S1 in the SI), close to the values reported in the literature for gaseous H_2S_2.[45]

The mixing of H_2S_2 (in $CHCl_3$) with $NOBF_4$ (in CH_3CN) led to an instantaneous formation of the new species with UV−vis absorbance at 358 nm (Figure 1A), different from 448 nm reported for $SSNO^-$.[24] This absorbance maximum was also quite shifted compared to the maximum observed for HSNO (338 nm).[16]

Cooled solutions of H_2S_2 and $NOBF_4$ were mixed and immediately sprayed using cryo-ESI (at −40 °C) into ultrahigh-

DOI: 10.1021/acs.inorgchem.5b00831
Inorg. Chem. XXXX, XXX, XXX−XXX

resolution TOF-MS. Several prominent peaks were observed, all of which corresponded to the HS_2NO species, with different numbers of solvent molecules. Because of the very low temperature ionization, formation of clusters with the solvent is expected (Figure 1B). More importantly, isotopic distribution of the signals is characteristic for the presence of two sulfur atoms (Figure S2 in the SI). While these results demonstrate that the product of the reaction between H_2S_2 and $NOBF_4$ is indeed HS_2NO, several structural isomers with this molecular formula could exist.

On the basis of the computational study, two structural motifs of the corresponding S_2NO^- anion seem to be thermodynamically accessible: $SSNO^-$ (in both the *cis*- and *trans*-$SSNO^-$ forms) and dithionitrate ($ON(S)S^-$) (Table S2 in the SI and Figure 1C). Interestingly, the extent of structural changes induced by a protonation is quite different in the case of these two isomers. Protonation of dithionitrate at either the oxygen or sulfur atom, which is energetically almost equally possible [with HON(S)S being only 2.2 kcal/mol less stable than HSN(O)S], does not cause any significant structural changes (Figure 1C). On the other hand, protonation of the terminal sulfur atom in the case of $SSNO^-$ (a thermodynamically most favorable protonation site in $SSNO^-$; Table S3 and Figure S3 in the SI) leads to a prominent elongation of the S−N bond, e.g., 1.953 Å (SCS-MP3/aug-cc-pVQZ) or 1.980 Å (SCS-MP3/aug-cc-pVTZ) in *cis*-HSSNO versus 1.676 Å (SCS-MP3/aug-cc-pVQZ) or 1.693 Å (SCS-MP3/aug-cc-pVTZ) in *cis*-$SSNO^-$ (Figure 1C and Figure S3 in the SI). Consequently, the calculated S−N bond dissociation energy for *cis*-HSSNO is only 16 kcal/mol (B3LYP/aug-cc-pVTZ+PCM), which is lower than that calculated for HSNO (27.3 kcal/mol). This points to an inherent instability of the protonated HSSNO species. The UV−vis spectral properties discussed above also implied that the protonated isomeric form present in the product solution does not contain the $SSNO^-$ structural moiety[24] ($SSNO^-$ or its protonated form, perthionitrous acid), speaking in favor of its dithionitric acid character.

In order to further clarify the structure of the obtained product we performed ^1H and ^{15}N NMR and in situ FTIR IR measurements. The solubility of $NOBF_4$ is highest in acetonitrile, but the solvent peak is then too strong to allow the measurement of ^{14}N NMR. Therefore, we used $^{15}NOBF_4$ as the reactant to obtain a ^{15}N NMR spectrum. The ^{15}N NMR measurements revealed two peaks with chemical shifts at +3 and +8 ppm (Figure 1D). This corresponds more to a nitrate-like (−4 ppm)[46] than *S*-nitroso-like structure (>400 ppm).[47] The appearance of the doublet is also indicative of two tautomeric structures [supposedly HON(S)S and HSN(O)S]. In addition, ^1H NMR of the $HS_2{}^{15}NO$ solution at −30 °C revealed a broad signal with a chemical shift of 9.2 ppm, reminiscent of the acidic proton (Figure S4 in the SI).

IR spectroscopy revealed the formation of a new species upon the addition of $NOBF_4$ into the solution of H_2S_2, characterized by vibrational frequencies at 1430, 1100, and 1054 cm^{-1} (Figure S5A in the SI). The latter two showed a shift toward lower frequencies when $^{15}NOBF_4$ was used. The observed isotopic shifts corresponded well to the calculated ones for the S−N bond: 1100 → 1073 cm^{-1} (calculated 1074 cm^{-1}) and 1054 → 1028 cm^{-1} (calculated 1027 cm^{-1}), as shown in Figure S5B in the SI. These values are in agreement with those reported for the double S=N bond in the case of 1,3,2,4-benzodithiadiazine.[48] In addition, no characteristic N=O bond vibration (expected for the HSSN=O isomer) could be observed. On the basis of all of these results, we proposed that the isomer formed in the reaction of H_2S_2 with $NOBF_4$ in an organic solvent has the character of dithionitric acid HON(S)S/HSN(O)S.

HS_2NO Having No Biological Effects Different from Those of Polysulfides. Furthermore, we were interested in the potential physiological importance of the product of the reaction between H_2S_2 and $NOBF_4$. We first tested the ability of this HS_2NO species to react with free thiols. Neither mercaptopropionate, as shown in Figure S6 in the SI, nor thiolphenol (data not shown) reacted with the reaction mixture of H_2S_2 and $NOBF_4$ to form characteristic *S*-nitrosothiol. This suggested that this reaction product cannot serve as an *S*-nitrosating agent, in accordance with the proposed HON(S)S/HSN(O)S structure. To test the ability of this HS_2NO species to act as a signaling molecule, we treated BAECs with HS_2NO made by the in situ mixing of H_2S_2 with $NOBF_4$ in acetonitrile. In the control experiments, we treated the cells with either the same volume of acetonitrile alone, H_2S_2 in acetonitrile, or $NOBF_4$ in acetonitrile. Cells were then analyzed for the levels of cGMP and cAMP. Despite the anticipated instability and very short lifetimes of H_2S_2 and $NOBF_4$ in aqueous solutions, both substances induced a small rise in the intracellular cGMP levels (Figure 2A). However, the addition of the H_2S_2 + $NOBF_4$ reaction mixture did not cause any further change compared to H_2S_2 alone. The effect on cAMP was opposite, and both H_2S_2 and the reaction mixture induced similar drops of the cAMP level (Figure 2B). $NOBF_4$ caused an expected increase of cGMP because it is the *S*-nitrosating agent and therefore could lead to the formation of NO-releasing

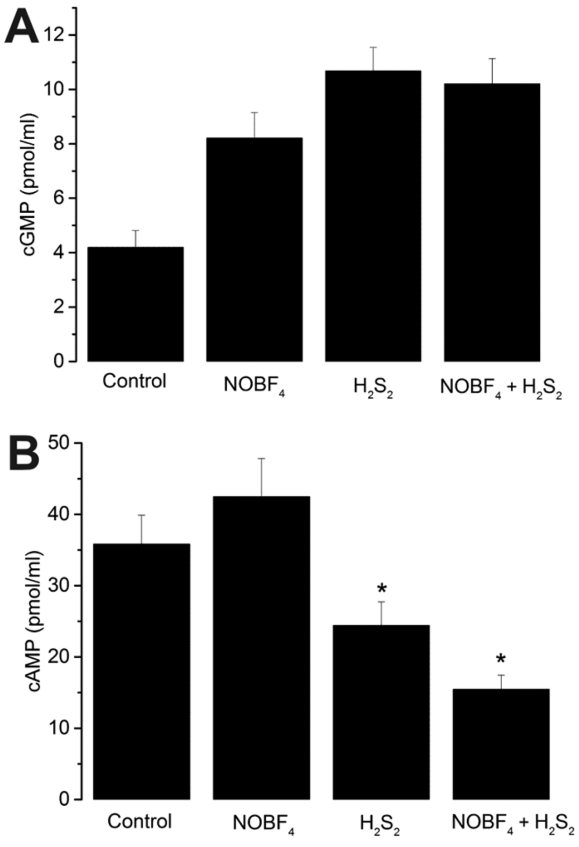

Figure 2. cGMP (A) and cAMP (B) levels in BAECs treated with a reaction mixture of H_2S_2 and $NOBF_4$.

DOI: 10.1021/acs.inorgchem.5b00831
Inorg. Chem. XXXX, XXX, XXX−XXX

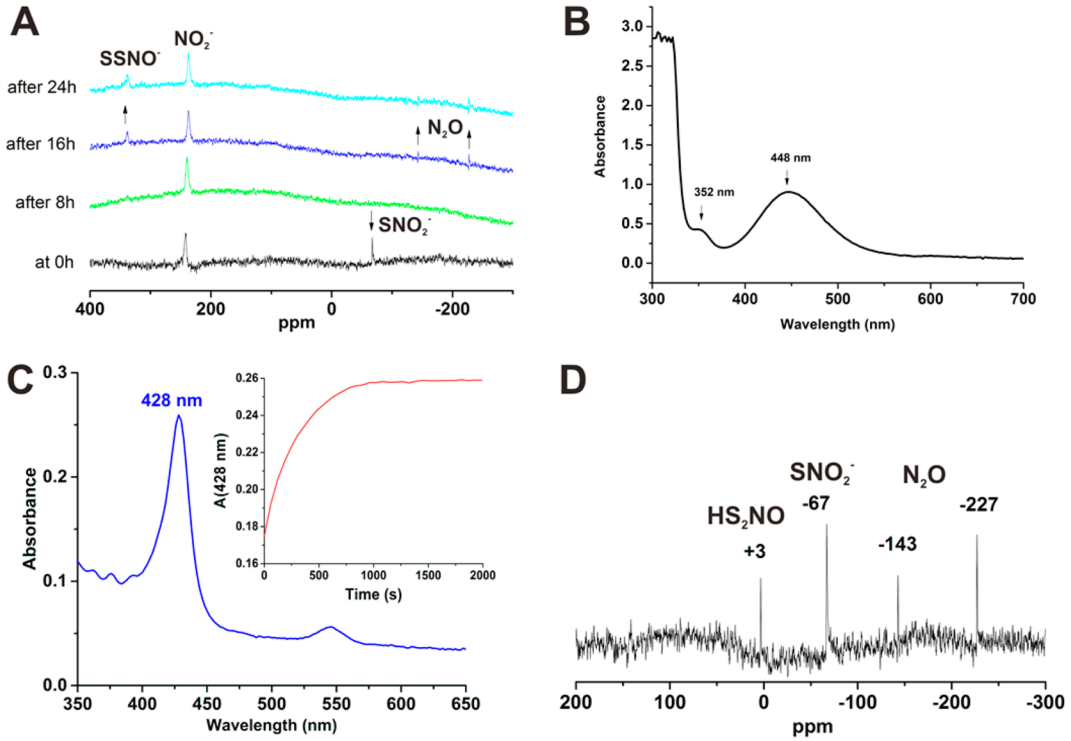

Figure 3. Formation of $SSNO^-$ from elemental sulfur and $PNP^+NO_2^-$ in acetone. (A) Reaction monitored by ^{15}N NMR. The measurement was performed at room temperature using a total number of 2878 scans with a relaxation delay of 0.4 s and a total recording time of 59 min. A 90° pulse was used. For clarity, only the spectra at 8 h increments are shown. (B) UV−vis spectrum of the reaction mixture (100 times diluted reaction mixture obtained as described in the Experimental Section) 24 h after the reaction was initiated. (C) UV−vis spectrum of the reaction mixture containing the diluted sulfur solution and an excess of $PNPNO_2$ (inset: time-dependent formation of a species followed at 428 nm). (D) ^{15}N NMR spectra of the reaction mixture of sulfur and $PNP^+NO_2^-$ in acetone irradiated for 3 days.

compounds.[20] Since polysulfides became recognized as molecules that could convey H_2S signaling, the rise of cGMP levels induced by H_2S_2 was also expected.[49,50]

If the obtained HS_2NO species was indeed a NO donor, the rise of cGMP should have been several-fold higher. However, the observed effects are comparable to those of H_2S_2, suggesting that its decomposition probably results in some sort of sulfane sulfur-containing compounds.

Synthesis and Chemical Characterization of PNP^+SSNO^-. The formation of $SSNO^-$ salts was reported in the literature in the reaction of elemental sulfur with $PNP^+NO_2^-$ in acetone.[24] We wanted to further study this reaction and characterize its product. The reaction was performed in an argon box with <1 ppm of H_2O and <1 ppm of O_2 using an ultra-dry acetone solution. Immediately after the addition of ^{15}N nitrite into an acetone solution of elemental sulfur, two ^{15}N NMR signals were observed, one at −67 ppm and the peak of unreacted nitrite at 241 ppm (Figure 3A). During the course of the reaction, the intermediate peak at −67 ppm disappeared and the formation of a new species with a chemical shift at 348 ppm (assigned to $SSNO^-$), together with the formation of N_2O (with chemical shifts at −143 and −226 ppm),[17] was observed. The signal at 348 ppm reached a maximum intensity after 24 h (Figure 3A).

The color change caused by the addition of $PNP^+NO_2^-$ into the acetone solution of sulfur was imminent, leading to the slow, time-dependent formation of a brownish-red solution and an insoluble sulfur oxidation product. UV−vis spectral characteristics of the reaction mixture were similar to those previously reported, with two prominent peaks at 352 and 448 nm, with the latter being assigned to the actual $SSNO^-$ anion (Figure 3B). However, when the reaction was performed with a diluted sulfur solution, a very different spectral change was observed (Figure 3C) that corresponded to the time-dependent formation of a species with an absorption maximum at 428 nm (Figure 3C, inset). We have recently experimentally observed and calculated the same absorption maximum for the sulfinyl nitrite HS(O)NO species in organic solvents, that is, an isomer of thionitrate ($HSNO_2$).[13] Seel et al. suggested that the most probable mechanism for the $SSNO^-$ formation involves the intermediate formation of SNO_2^- and its subsequent disproportionation to $SSNO^-$ and NO_3^- (eqs 4 and 5).[24]

$$S + NO_2^- \rightarrow SNO_2^- \quad (4)$$

$$2SNO_2^- \rightarrow SSNO^- + NO_3^- \quad (5)$$

The initial attack of a nitrogen lone pair on the electrophilic sulfane sulfur in solvents such as acetone or *N*,*N*-dimethylformamide (DMF) could indeed lead to the intermediate formation of SNO_2^-. The signal at −67 ppm in ^{15}N NMR and the peak at 428 nm in the UV−vis absorbance spectrum could therefore be assigned to SNO_2^- (eq 4). However, the absence of any nitrate signal in the ^{15}N NMR spectra excludes the second reaction step (eq 5). As an alternative, a further reaction of SNO_2^- with sulfane sulfur can lead to the formation of $SSNO^-$ and probably oxidized sulfur species of unidentified structure, which precipitates from the solution (eq 6):

$$S_x + SNO_2^- \rightarrow SSNO^- + S_{x-1}O \quad (6)$$

DOI: 10.1021/acs.inorgchem.5b00831
Inorg. Chem. XXXX, XXX, XXX−XXX

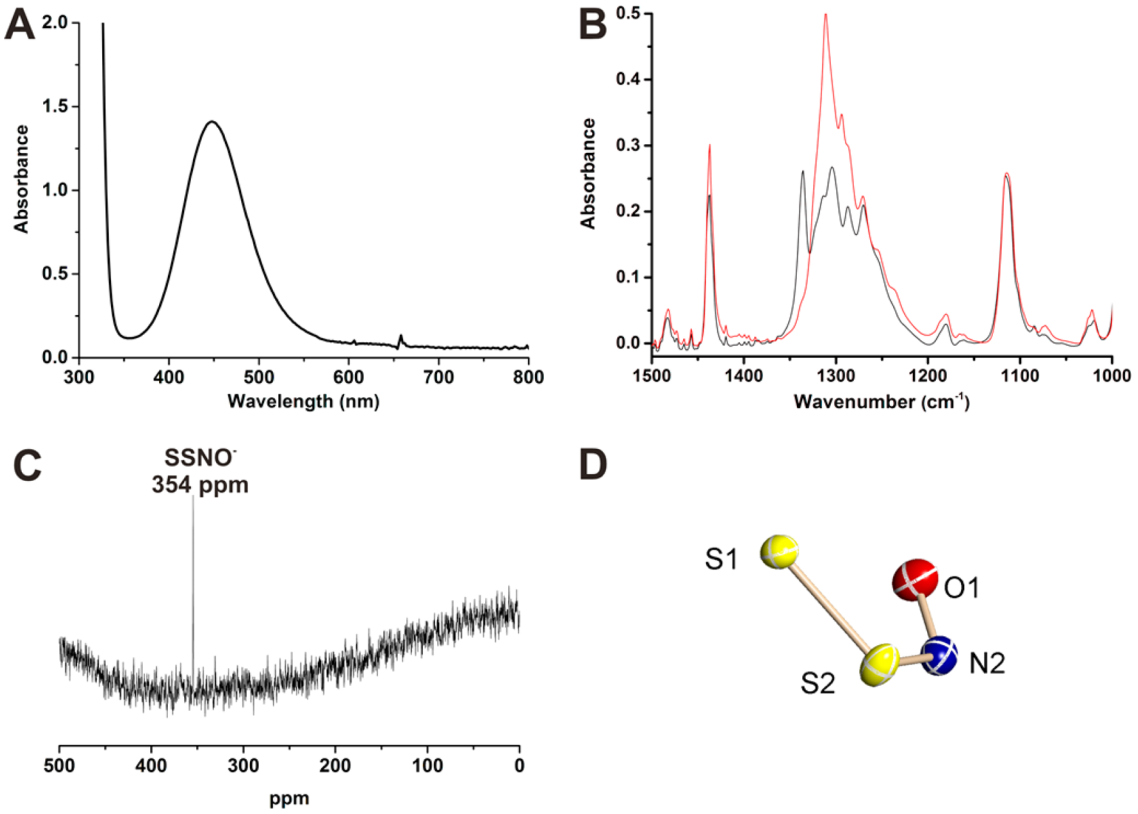

Figure 4. Chemical characterization of PNP^+SSNO^-. (A) UV−vis spectrum of 450 μM PNP^+SSNO^- in acetone. (B) FTIR spectra of $PNP^+SS^{14}NO^-$ (black) and $PNP^+SS^{15}NO^-$ (red). (C) ^{15}N NMR spectrum of PNP^+SSNO^- in acetone. (D) ORTEP drawing for PNP^+SSNO^-, showing carbon atoms as gray, phosphorus as pink, nitrogen as blue, oxygen as red, and sulfur as yellow and the 50% probability ellipsoids for non-hydrogen atoms.

This would match nicely with our observation that there was no further transformation of SNO_2^- in solution (inset in Figure 3C) that contained excess of $PNP^+NO_2^-$ because there was not enough sulfane sulfur for the reaction shown in eq 6.

The formation of N_2O (Figure 3A) suggests that formed $SSNO^-$ could further decompose. Indeed, irradiation of the reaction mixture, monitored by ^{15}N NMR, led to the much stronger N_2O formation (Figure S7A in the SI). Irradiation (LED stick; 470 nm; 51.1 ± 1.0 mW) of the diluted reaction mixture followed by UV−vis spectra led to the complete disappearance of the $SSNO^-$ absorbance maximum, followed by the rise of the peak at 354 nm (Figure S7B in the SI), characteristic for dithionitrate (the "H_2S_2 + $NOBF_4$" reaction product; Figure 1A). A partial $SSNO^-$ (photo)isomerisation to dithionitrate $[SN(S)O^-]$ was also evidenced by the appearance of the signal at +3 ppm in the ^{15}N NMR spectrum (Figure 3D; for comparison, see Figure 1D) of the reaction mixture irradiated for 3 days (to achieve complete $SSNO^-$ decomposition like in the experiment with the diluted reaction mixture). This spectrum (Figure 3D) also confirmed the presence of N_2O as the decomposition product, as well as a photoinduced SNO_2^- formation (−67 ppm), which formally represents a reverse of the reaction equation (6).

Once formed in the solution, PNP^+SSNO^- could be crystallized and subsequently characterized. Crystals of both $PNP^+SS^{14}NO^-$ and $PNP^+SS^{15}NO^-$ were prepared, the latter for the FTIR and ^{15}N NMR measurements. Because of the coformation of the insoluble sulfur species, the solution was recrystallized several times to obtained dark-red-brown crystals (occasionally with a few yellow crystals). When dissolved in acetone, PNP^+SSNO^- has only one characteristic absorption maximum at 448 nm (Figure 4A) with an extinction coefficient of 3125 M^{-1} cm^{-1} (Table 1). FTIR spectra showed a broad band centered at ∼1300 cm^{-1}, split into four bands at 1335, 1304, 1297, and 1271 cm^{-1}, all of which shifted to lower wavenumbers when $PNP^+SS^{15}NO^-$ was used (Figure 4B and Table 1). In the ^{15}N NMR spectrum, only one signal at 354 ppm was present (Figure 4C and Table 1), in agreement with the product species that we observed during the course of the reaction between nitrite and elemental sulfur (Figure 3A).

Table 1. Physicochemical Characteristics of PNP^+SSNO^-

UV−vis	448 nm (ε_{448} = 3125 M^{-1} cm^{-1})	
FTIR		
$SS^{14}NO^-$ (ν_{NO}, cm^{-1})	1335, 1304, 1297, 1271	
$SS^{15}NO^-$ (ν_{NO}, cm^{-1})	1311 (calcd 1311), 1286 (calcd 1281), 1270 (calcd 1273), 1254 (calcd 1251)	
^{15}N NMR	δ 354 ppm	
	Crystal Structure	
	yellow crystals	red crystals
	Angles (deg)	
S1−S2−N	115.2(2)	115.1(2)
S2−N−O	117.8(4)	117.8(2)
	Bond Lengths (Å)	
S1−S2	1.974(2)	1.9750(9)
S2−N	1.700(6)	1.696(3)
N−O	1.242(6)	1.246(3)

DOI: 10.1021/acs.inorgchem.5b00831
Inorg. Chem. XXXX, XXX, XXX−XXX

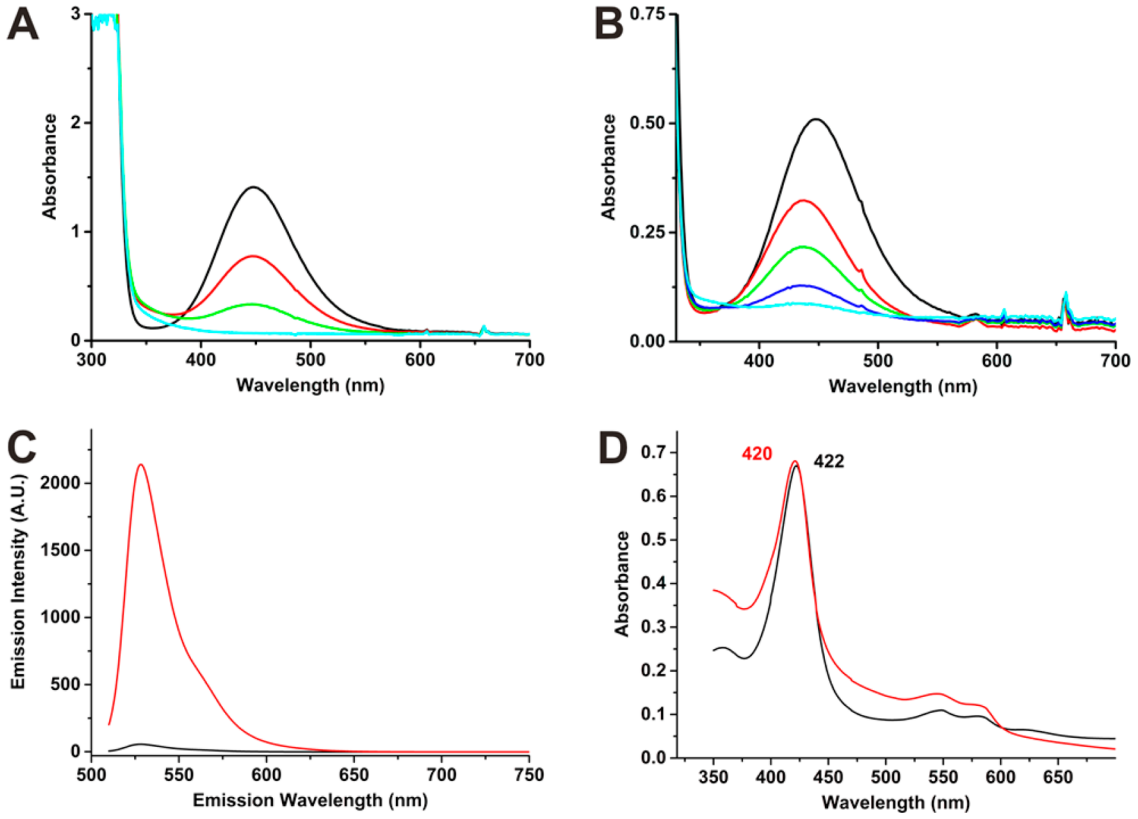

Figure 5. Decomposition of PNP^+SSNO^-. (A) 500 μM PNP^+SSNO^- acetone solution (black) irradiated for 5 s (red line), 10 s (green line), and 15 s (blue line). (B) Spectra of 200 μM PNP^+SSNO^- acetone solution (black) into which 10% water was added (red) and the change monitored 10 s (green), 100 s (dark blue), and 10 min later (light blue). (C) Changes in fluorescence spectra of 10 μM CuBOT1 (black) in a 50 mM potassium phosphate buffer 10 min after the addition of 20 μM PNP^+SSNO^- (red). (D) Comparison of the UV−vis spectra obtained by mixing 10 μM deoxymyoglobin (black) or metmyoglobin (red) with 10 μM PNP^+SSNO^- in a 50 mM potassium phosphate buffer. The black spectrum corresponds to the Fe^{2+}-HNO myoglobin, while the red spectrum corresponds to the Fe^{2+}-NO myoglobin spectrum.

Finally, single-crystal structure determinations were performed. Two types of crystals were isolated, dark-red-brown and yellow crystals. Both have been analyzed to show the same structure (Figure 4D and Tables S1−S3 in the SI). The observed bond distances in the $SSNO^-$ anion (Table 1) show slight differences from what was previously reported,[24] but considering the obtained estimated standard deviation values, the differences are not significant with regard to the crystallographic 3σ criterion. The bond distances observed in our structure determinations are in good agreement with our calculated *cis*- and *trans*-$SSNO^-$ geometries [Figures S3 in the SI (SCS-MP3/aug-cc-pVTZ) and 1C (SCS-MP3/aug-cc-pVQZ)]. Further comparisons indicate that the N−O and S−N bonds are longer than the typical N═O bond found in *S*-nitrosothiols[51] and the S−N in poly(sulfur nitride) (163 pm),[52] respectively, whereas the S−S bond is somewhat between that of S_2 (189 pm) and H_2S_2 (205 pm).[53]

The bond lengths reported herein (Table 1) are indicative of an overall delocalization of the negative charge and even imply a slightly polarized S_2---NO^--like structure. A calculated gas-phase Mulliken charge distribution reveals a prominent negative charge at the NO moiety ($[S_2^{-0.39}$---$NO^{-0.61}]^-$ and $[S_2^{-0.31}$---$NO^{-0.69}]^-$ charge distribution patterns within *cis*- and *trans*-$SSNO^-$, respectively; Table S4 in the SI). Such an electronic structure is supported by the low vibration frequency for the N═O bond (Table 1). The literature values for the vibration frequency of the N═O bond in typical *S*-nitrosothiols are in the 1500−1600 cm^{-1} range (1569 cm^{-1} for HSNO).[16] Lower vibration frequency implies a stronger HNO character of the NO unit in $SSNO^-$. These structural features are, therefore, indicative of its chemical nature being different from that expected for the *S*-nitrosothiols. In fact, the observed values for $SSNO^-$ are even lower than that for the free NO^- (1363 cm^{-1})[54] and identical with those found for coordinated HNO in some six-coordinate $\{M(HNO)\}^8$ complexes.[55] By way of comparison, ν_{NO} in $Re(Cl)(CO)_2(Pcy_3)_2(HNO)$ and [Fe-(cyclam-ac)NO] is at 1335 and 1271 cm^{-1},[56,57] respectively, whereas for $[Ru(Me_3[9]aneN_3)(bpy)NO]^+$, two ν_{NO} vibrations at 1315 and 1286 cm^{-1} are reported.[58]

$SSNO^-$ Is Intrinsically Unstable and Decomposes To Give Sulfur and HNO. In their papers, Kortese-Crott et al. claimed that the stable reaction product between *S*-nitrosothiols and H_2S in water is the yellow $SSNO^-$ species, which can be purified by column chromatography and which slowly decomposes in the cells to give NO.[21,23] To test the actual stability of $SSNO^-$, the PNP salt was dissolved in acetone and the stock solutions were kept in dark vials, protected from light. Exposure to light (LED stick; 470 nm; 51.1 ± 1.0 mW) led to the fast and complete decomposition of $SSNO^-$ (Figure 5A). The addition of 10% water into an acetone solution of PNP^+SSNO^- caused equally fast decomposition and complete loss of the characteristic absorbance maximum (Figure 5B).

As discussed above, $SSNO^-$ possesses a quite long S−N bond, which becomes even further elongated upon protonation (Figures 1C and S3 in the SI). Furthermore, the negative charge is somewhat more distributed over the NO moiety, in

DOI: 10.1021/acs.inorgchem.5b00831
Inorg. Chem. XXXX, XXX, XXX−XXX

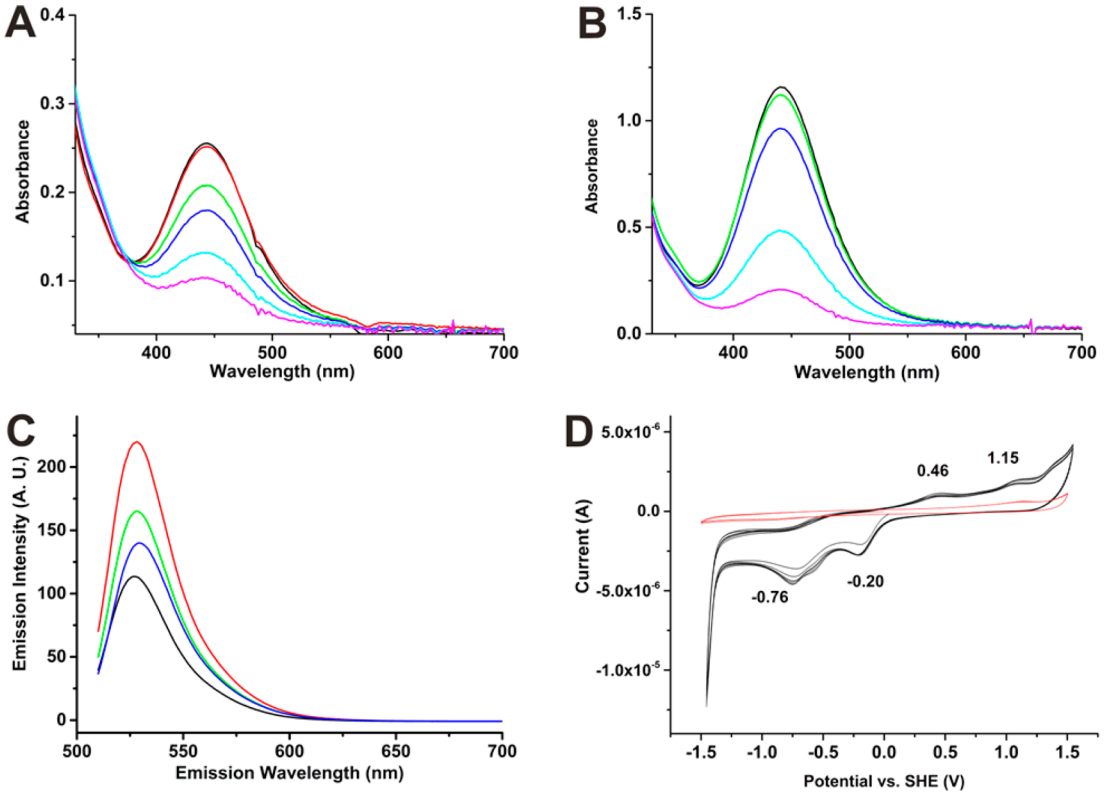

Figure 6. Reactivity of $SSNO^-$ toward biologically relevant molecules. (A) Time-resolved absorbance spectra of the reaction of allyl mercaptan (6 mM in acetonitrile) with $SSNO^-$ (82 μM in acetone) before mixing (black line), immediately after mixing (red line), after 30 s (green line), after 150 s (dark-blue line), after 450 s (light-blue line), and after 900 s (purple line). The decrease of the $SSNO^-$ peak at 448 nm is clearly visible. (B) Time-resolved absorbance spectra of the reaction of allyl disulfide (6 mM in acetonitrile) with $SSNO^-$ (370 μM in acetone) before mixing (black line), 30 s after mixing (green line), after 150 s (dark-blue line), after 450 s (light-blue line), and after 900 s (purple line). The decrease of the $SSNO^-$ peak at 448 nm is clearly visible. (C) Changes in fluorescence spectra of 10 μM DHR (black line) in acetone upon the successive addition of 100 μM H_2O_2 (red line), 2 mM $SSNO^-$ (green line), and finally another 2 mM $SSNO^-$ (blue line) into the same cuvette. $SSNO^-$ is able to partially reduce RH 123 formed upon DHR oxidation with H_2O_2. (D) Cyclic voltammogram of a 2 mM PNP^+SSNO^- solution in acetone (black line) compared to a cyclic voltammogram of the solvent alone (red line). The scans shown were performed with a rate of 0.1 V/s starting from 0 to −1.5 to +1.5 V and back, referred to the silver wire used. Voltammograms are presented referring to SHE; ferrocene was used as additional potential reference.

both the anionic and protonated HSSNO forms (Table S4 in the SI). Thus, it should be expected that the protonation-induced $SSNO^-$ decomposition should lead to sulfur and NO^-/HNO formation. In fact, the water addition leads to the immediate formation of elemental sulfur (Figure S8 in the SI).

Detection of HNO requires several methodological approaches in order to differentiate NO from HNO. We first used DAF-FM for detection of the decomposition product(s) of $SSNO^-$. The addition of PNP^+SSNO^- into a buffered DAF-FM solution leads to the immediate rise of the characteristic fluorescence (Figure S9A in the SI). Although widely used as a NO sensor, DAF-FM does not react with NO itself but rather with N_2O_3. In addition, DAF-FM readily reacts with HNO as well.[59] We therefore used an electron paramagnetic resonance (EPR) method by applying Fe^{2+}-DETC and Fe^{3+}-DETC (formed in situ) as scavengers to differentiate between NO and HNO. Indeed, the characteristic EPR spectrum of a mononitrosyl complex with $g_{||}$ = 2.021 was only observed when Fe^{3+}-DETC was mixed with PNP^+SSNO^-,[31,32] suggesting that the decomposition product is HNO (Figure S9B in the SI). Further confirmation of the HNO formation came from the experiments involving the use of a copper-based HNO fluorescence sensor (CuBOT1).[28] The addition of PNP^+SSNO^- led to the immediate reduction of Cu^{2+} and an increase of the fluorescence (Figure 5C). Finally, to exclude the possibility of the concomitant release of NO, we added PNP^+SSNO^- into a buffered solution of deoxymyoglobin and metmyoglobin. Farmer and co-workers demonstrated that when HNO reacts with deoxymyoglobin, it forms a HNO−Fe^{2+}Mb complex, whose UV−vis spectral properties differ from the product of metmyoglobin with HNO (which is identical with the product of deoxyhemoglobin with NO).[60,61] Indeed, the observed Soret band shift was identical with the one reported in the literature[60,61] (Figure 5D). Furthermore, the complete transformation of deoxymyoglobin to HNO−Fe^{2+}Mb was observed when equimolar concentrations of deoxymyoglobin and PNP^+SSNO^- were mixed. This implies that the entire amount of $SSNO^-$ immediately decomposes upon the addition into water to give HNO.

Protonation of $SSNO^-$ by the addition of acid into an acetone solution also led to its immediate decomposition, while the addition of NaOH pellets or dried triethylamine showed no significant loss of $SSNO^-$ (data not shown).

Even without protonation, the molecule seems to be intrinsically unstable. We already observed that the ^{15}N NMR signal of $SSNO^-$ is always accompanied by signals belonging to N_2O (Figure 3A). HNO dimerizes fast with elimination of water to give N_2O.[62] In addition, mixing $SSNO^-$ with the iron(III) *meso*-tetraphenylporphyrinato [Fe^{3+}(TPP)] complex in an aprotic medium led to the immediate formation of the

DOI: 10.1021/acs.inorgchem.5b00831
Inorg. Chem. XXXX, XXX, XXX−XXX

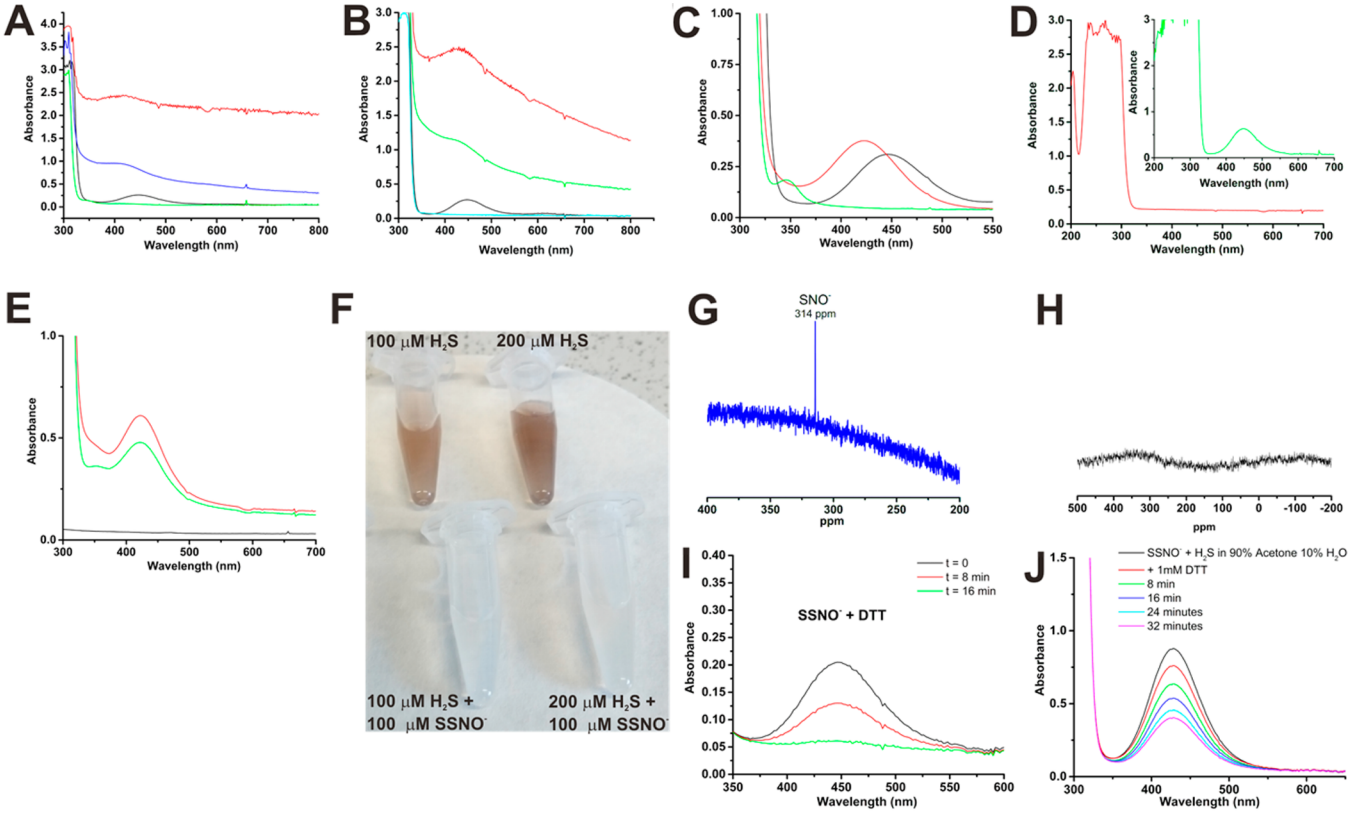

Figure 7. Reaction of $SSNO^-$ with sulfide. (A) 100 μM PNP^+SSNO^- acetone was mixed, in a tandem cuvette, with 2 mM Na_2S in water (1:1, v/v). The black line is the spectrum before mixing and the red line that immediately after mixing. The blue line is the spectrum after centrifugation of the reaction mixture (~5 min after the reaction was started); the green line is the spectrum after further filtration (~90 min after the reaction was started). (B) Addition of 100 μL of Na_2S dissolved in water (final concentration 2 mM) into 900 μL of 100 μM PNP^+SSNO^- in an acetone solution. The black line is the spectrum of PNP^+SSNO^- before the addition of Na_2S and the red line that immediately after Na_2S was added. The green line is the spectrum of the reaction mixture after 5 min of centrifugation and the blue line that after further filtration through a 2 μm PTFE syringe filter. (C) Concentrated PNP^+SSNO^- was mixed with Na_2S in a 1:10 molar ratio, filtered, and diluted further (red line). The species at ~420 nm decomposes completely after 90 min (green spectrum). For comparison, the spectrum of an untreated but in the same way processed solution of PNP^+SSNO^- in acetone is shown in black. (D) Addition of PNP^+SSNO^- into a 300 mM phosphate buffer (pH 7.4) to give a 200 μM final concentration (red spectrum). Inset: 200 μM PNP^+SSNO^- in acetone. (E) Addition of PNP^+SSNO^- into a 2 mM Na_2S solution [in a 300 mM phosphate buffer (pH 7.4)] to give a 200 μM final concentration (red spectrum). The spectrum of the reaction mixture after 7 min is shown in green, and the spectrum of 2 mM Na_2S in a 300 mM phosphate buffer (pH 7.4) prior to the addition of PNP^+SSNO^- is shown in black. (F) Detection of the remaining sulfide by $Pb(CH_3COO)_2$. Upper lane: Addition of 1 mM $Pb(CH_3COO)_2$ into the solutions containing 100 and 200 μM Na_2S in a 300 mM phosphate buffer (pH 7.4). Lower lane: Addition of 1 mM $Pb(CH_3COO)_2$ into the solutions immediately after 100 μM PNP^+SSNO^- was mixed with 100 and 200 μM Na_2S in a 300 mM phosphate buffer (pH 7.4). (G) ^{15}N NMR spectrum of the reaction mixture of Na_2S and $PNP^+SS^{15}NO^-$ in acetone (10% water). (H) ^{15}N NMR spectrum of the reaction mixture of Na_2S and $PNP^+SS^{15}NO^-$ in buffer (10% acetone). (I) Addition of 1 mM DTT into a 100 μM PNP^+SSNO^- solution in acetone: (black) before the addition; (red) 8 min after the addition; (green) 16 min after the addition. (J) Addition of 1 mM DTT into a filtered reaction mixture of PNP^+SSNO^- and Na_2S (90% acetone and 10% H_2O) and the spectra recorded every 8 min.

low-spin Fe^{2+}-NO complex, as determined by the EPR (Figure S10 in the SI), which confirms the NO^- generation upon spontaneous $SSNO^-$ decomposition.

Redox Properties of $SSNO^-$: Reactivity with Biologically Relevant Molecules. We then focused on examining the reactivity of $SSNO^-$ with thiols in acetone solutions. For this, we used cysteine methyl ester and cystin dimethyl ester (Figure S11A,B in the SI) as well as allyl mercaptan and allyl disulfide (Figure 6A,B). To our surprise, $SSNO^-$ reacted with both oxidized and reduced thiols, as characterized by the loss of the 448 nm absorbance peak. Furthermore, it appears that the reaction with oxidized thiols is even faster than that with the reduced ones (Figure S11C in the SI), suggesting that $SSNO^-$ is better reducing than the oxidizing agent. We further probed its reactivity toward DHR. Oxidation of DHR generally leads to the formation of rhodamine 123 (RH 123) with characteristic fluorescence.[63] DHR is prone to oxidation, and even the stock solution contains a small percentage of oxidized RH 123. When $SSNO^-$ was added into a DHR solution in acetone, it led to a decrease of the basal fluorescence, suggesting that $SSNO^-$ can reduce oxidized DHR (Figure S11D in the SI). To confirm this, we oxidized DHR to RH 123 by adding an excess of H_2O_2. This led to an increase of the fluorescence. The subsequent addition of $SSNO^-$, however, reduced RH 123 back to DHR (Figure 6C).

$SSNO^-$ could be considered as a thiol-based analogue of peroxynitrite, which acts as an oxidant and can oxidize phenols, in general, and tyrosine residues in proteins, in particular, forming dityrosine.[64] To test whether $SSNO^-$ exhibits the same reactivity, we mixed it with phenol and measured the fluorescence signal of diphenol formation. While peroxynitrite

DOI: 10.1021/acs.inorgchem.5b00831
Inorg. Chem. XXXX, XXX, XXX−XXX

caused phenol oxidation, $SSNO^-$ failed to cause any change (Figure S11E,F in the SI).

The cyclic voltammetry measurements revealed that $SSNO^-$ could indeed be oxidized and reduced. The irreversible reduction waves appeared at −0.20 and −0.76 V (SHE), while the irreversible oxidation waves appeared at +0.62 and +1.15 V (SHE) (Figure 6D). Because of the fact that the highest occupied molecular orbital (HOMO) of $SSNO^-$ has a bonding and the lowest unoccupied molecular orbital (LUMO) an antibonding character (Figure S12 in the SI), it is expected that both oxidation and reduction will destabilize the molecule, probably resulting in its decomposition, which explains the irreversible nature of the observed redox processes.

The potentials of −0.76 and +1.15 V correspond well to the standard redox potentials for the NO/NO^- and NO^+/NO redox couples, respectively.[65,66] Therefore, one electron reduction of $SSNO^-$ probably proceeds by the following equation:

$$SSNO^- + e^- \rightarrow NO + S_2^{2-} \quad (7)$$

The observed value of −0.20 V is in the range of the values observed for the $RSNO/RS^-$, NO redox couples.[67] The generation of NO, which is then reduced to NO^-, can explain the second reduction peak at −0.76 V.[65]

The oxidation probably proceeds as observed for the $ONOO^\bullet/ ONOO^-$ redox couple:

$$SSNO^- - e^- \rightarrow SSNO^\bullet \quad (8)$$

The measured value of +0.46 V is quite similar to the values calculated and measured for the $ONOO^\bullet/ONOO^-$ redox couple.[68] The subsequent fate of $SSNO^\bullet$ is difficult to predict, but the following oxidation wave at +1.15 V suggests that $SSNO^\bullet$ might further decompose to give S_2 and NO, which then oxidizes to NO^+ at ∼1.2 V.[66] Interestingly, unlike $ONOO^-$, which almost exclusively acts as an oxidizing agent, $SSNO^-$ seems to exhibit a reducing rather than an oxidizing chemistry.

$SSNO^-$ Cannot Cause S-Nitrosation or S-Sulfhydration of Proteins under Physiological Conditions. Despite its instability on light and in water, we tested the ability of PNP^+SSNO^- to modify proteins when added into a buffered solution. GAPDH and BSA were used as model proteins because they are known to be both S-nitrosated and S-sulfhydrated.[34] We used the biotin-switch method do detect *S*-nitrosothiol formation and modified the tag-switch method to detect S-sulfhydration. PNP^+SSNO^- (24 mM final concentration) was added into a buffered solution containing GAPDH (27.7 μM) or BSA (40 μM) and incubated for 5 or 30 min in the dark or with irradiation. However, no transnitrosation or persulfidation was observed (not shown). This once again confirmed that $SSNO^-$ cannot serve as a signaling molecule involved in these protein post-translational modification, let alone as a long-lasting storage of NO under physiological conditions, different from what has been suggested in the literature.[21−23]

$SSNO^-$ Reacts with Sulfide To Give SNO^-. The only argument in the literature for the $SSNO^-$ formation in the reaction of sulfide and *S*-nitrosothiols is the observation that the final yellow product shows the absorbance shift from 412 to 448 nm when mixed with organic solvents such as dimethyl sulfoxide, DMF, etc.[21−23] This product is stable for hours and could slowly release NO.[21,22] In addition, a suggestion appeared recently that $SSNO^-$ might be stabilized under physiological conditions by an excess of H_2S.[22,23] We have shown previously, studying the reaction of *S*-nitrosothiols with H_2S, that this yellow product remains long after the ^{15}N NMR signal from HSNO disappears (with the only remaining NMR signal being that of nitrite), which led us to propose that this is some mixture of polysulfides,[16] but it could as well be a mixture of aqueous sulfur sols (particles consisting of a sulfur core surrounded with oxidized polysulfides).[69] In addition, we also demonstrated recently that a similar yellow product could be observed when H_2S was mixed with superoxide and that its absorbance maxima show the same hypsochromic shift, which is assigned to $S_2^{\bullet-}/S_4^{2-}$.[15]

In the light of the data presented herein, it is obvious that $SSNO^-$ is intrinsically unstable and decomposes easily as well as that it readily reacts with other thiols. We therefore wanted to test whether $SSNO^-$ reacts further with H_2S or it is stabilized by its presence. The reaction of sulfide with $SSNO^-$ was initially studied by mixing the same volumes of Na_2S solution in water with PNP^+SSNO^- in acetonitrile (Figure 7A). Immediate precipitation occurred, which led to light scattering, followed by the appearance of a new absorbance peak at ∼420 nm. Centrifugation improved the quality of the spectrum, but the formation of a precipitate continued. After the reaction mixture was filtered through a 2 μm PTFE syringe filter, the 420 nm peak disappeared. Similar solution behavior was observed when Na_2S was added to introduce only 10% water to the acetone solution of PNP^+SSNO^- (Figure 7B). When working with a much more concentrated solution of PNP^+SSNO^-, we could nicely isolate the spectrum of the newly formed species after filtration, which shows the absorbance maximum at ∼420 nm. However, the peak decayed steadily and completely disappeared after 60 min, with the concomitant appearance of a new peak at 345 nm (suggestive of $HSNO/SNO^-$; Figure 7C).

To prove that the observed 420 nm peak is not the peak of $SSNO^-$ dissolved in water, we added PNP^+SSNO^- (stock solution made in acetone) to a 50 mM phosphate buffer (pH 7.4) to yield a 200 μM final concentration of $SSNO^-$ (and 10% of the final acetone concentration). No absorbance maximum in the visible spectrum could be observed (Figure 7D). However, when the same concentration of PNP^+SSNO^- was added into a 50 mM phosphate buffer (pH 7.4) containing 2 mM H_2S, the appearance of 420 nm peak was observed immediately after the mixing (Figure 7E), although some light scattering could be observed as well because of insoluble particle formation. Finally, we tested what happens with H_2S from the solution. To the phosphate buffer (pH 7.4) containing 100 and 200 μM sulfide was added PNP^+SSNO^- to yield a 100 μM final concentration. The presence of sulfide was qualitatively assessed immediately after the mixing (∼30 s) by the addition of a 1 mM lead acetate solution. In both cases, there was no characteristic formation of insoluble PbS, as opposed to the control samples of the same H_2S concentration where $SSNO^-$ was not added (Figure 7F). This clearly indicates that H_2S reacts with $SSNO^-$ in a ratio that is probably higher than 2:1.

^{15}N NMR analysis of the reaction mixture containing $PNP^+SS^{15}NO^-$ and Na_2S (final amounts: 90% acetone, 10% H_2O, v/v) revealed the presence of only one signal with a chemical shift of 314 ppm (Figure 7G). The signal was observable even 4 h after the mixing, long after the 420 nm peak disappeared, while the peak characteristic for $HSNO/SNO^-$ was still present (Figure 7C). The chemical shift matches the one we observed for HSNO in the reaction of *S*-

DOI: 10.1021/acs.inorgchem.5b00831
Inorg. Chem. XXXX, XXX, XXX−XXX

nitrosoglutathione and H_2S (322 ppm).[16] The slight change is probably due to the fact that in our previous study we worked at pH 7.4, where HSNO existed in a protonated form, while in the experiments shown in Figure 7G, an aqueous solution of Na_2S was used, which is very alkaline and therefore the formation of deprotonated SNO^- is expected.

These experiments clearly demonstrate that $SSNO^-$ readily reacts with S^{2-}/HS^-:

$$SSNO^- + S^{2-} \rightarrow SNO^- + S_2^{2-} \quad (9)$$

Persulfide is unstable, as we showed here, leading to immediate sulfur precipitation, which explains the experimental results shown in Figure 7A,B.

However, this reaction occurs only when acetone is the main solvent (10% water). When the reaction was performed using the same concentrations but in 90% water and 10% acetone, no ^{15}N NMR signal could be observed (Figure 7H), although the solution does initially show a 420 nm peak (Figure 7E). This matches nicely with our experimental data presented here (Figures 5B–D and 7D) as well as with computational studies (Figure 1C), suggesting the instability of $SSNO^-$ in an aqueous solution. Under such experimental conditions, decomposition of $SSNO^-$ is the predominant process, leading to HNO generation and subsequent elimination of gaseous N_2O. S_2, as the other product, is unstable, so it is possible that this is the species that reacts further with H_2S in air to form aqueous sulfur sols.

While $SSNO^-$ reacts readily with thiols (Figures 6A,B and S11A,B in the SI) including dithiothreitol (DTT; Figure 7I), the species with a 420 nm absorption maximum is more resistant to DTT, reacting much slower (Figure 7J). This further supports the hypothesis of aqueous sulfur sols being species with 420 nm absorption maximum because they consist of the sulfur (the core of the particle) surrounded with oxidized polysulfides,[69] which would be less prone to DTT-induced cleavage than normal polysulfides.

Taken together, these data demonstrate the following:

(1) H_2S_2 reacts with NO^+ to give dithionitrate (or the corresponding dithionitric acid) rather than $SSNO^-$.

(2) $SSNO^-$ is unstable and decomposes when protonated or exposed to light.

(3) The structure and chemical reactivity of $SSNO^-$ suggest its S_2---NO^- character rather than the character of a typical *S*-nitrosothiol structure.

(4) When added into water/buffer, it decomposes to HNO and sulfur.

(5) $SSNO^-$ could be involved in both oxidation and reduction processes, as demonstrated by its reactivity toward reduced and oxidized thiols.

(6) $SSNO^-$ is not stabilized by the excess of sulfide; in fact, $SSNO^-$ readily reacts with sulfide, forming SNO^-, which is a more stable species than $SSNO^-$.

(7) The observed 420 nm peak is the product of the reaction between $SSNO^-$ and sulfide and does exist even in acetone, the solvent in which $SSNO^-$ shows an absorption maximum at 448 nm.

(8) A 420 nm peak is also formed when the reaction between $SSNO^-$ and sulfide is performed in water; sulfide is almost completely consumed under these conditions even when $SSNO^-$ and H_2S are mixed in a 1:2 ratio, but no HSNO could be detected.

(9) $SSNO^-$ decomposed in the presence of DTT, while the 420 nm species reacts much slower, suggesting that these might be aqueous sulfur sols.

Conclusion: SNO^-/HSNO versus $SSNO^-$/HSSNO and Implications for the Biological Activity and Cell Signaling. The herewith-performed experiments revealed inherent instability of $SSNO^-$ even in aprotic media and high instability upon protonation. Its isomer dithionitrate $[SN(O)S^-]$ does not undergo a prominent structural change upon protonation (Figure 1C) and consequently can be detected in the form of dithionitric acid in organic solvents. On the other hand, HSNO can exist as such in aqueous solutions and was detected in its protonated form $\{HSNO + H^+\}$ under MS experimental conditions.[16] Our computational data clearly support a difference in the stability of HSSNO and HSNO by demonstrating the significantly elongated S–N bond (e.g., 1.953 or 1.980 Å; Figures 1C and S3 in the SI) in HSSNO compared to that in HSNO (1.86 Å), making it more prone to cleavage.[16,70]

Our previous studies have shown that HSNO can generate HNO in the reaction with H_2S.[16] A mechanism of this reaction has recently been studied by DFT in the literature. It has been shown that S–N bond cleavage in HSNO can occur only upon S–S bond formation in the water-assisted reaction of H_2S/HS^- with the *y* isomer of HSNO.[70] Importantly, the S–N bond in $SSNO^-$ is already longer (Table 1) than the corresponding bond in the predicted $\{HSSN(H)O\}^-$ transition state (1.67 Å), which led to HNO and H_2S_2.[70] On the basis of that comparison, it could argued that, in a protic medium, $SSNO^-$ has more transient than intermediate character. Therefore, it is expected that, in the presence of water/protons, the S–N bond in protonated $SSNO^-$ is highly activated toward its cleavage, resulting in this case in HNO and elemental sulfur (initially S_2). Furthermore, experimental data clearly show that $SSNO^-$ reacts readily with sulfide to form $HSNO/SNO^-$, supporting the predominant role of the latter in any biological context (Figure 7).

In terms of the biological effects, we have shown that HSNO can have a role as a molecular shuttle for the NO^+ unit and as such is involved in trans-S-nitrosation of proteins.[16] On the contrary, structural and electronic features, as well as the observed reactivity of $SSNO^-$, do not support its direct NO^+- or NO-donating ability. It can rather serve as a fast HNO-releasing agent, which in our future studies will be tested in biological systems. Though its decomposition also results in elemental sulfur, we have not found evidence that it can induce persulfidation of proteins. On the basis of its overall inherent instability, the generation of $SSNO^-$ under physiological conditions is highly unlikely, even as a reactive intermediate within hydrophobic cellular environments. If at all, the formation of other isomeric forms, dithionitrate or the corresponding dithionitric acid, seems to be more likely. However, the extreme instability of H_2S_2, required for its generation in a reaction with some NO^+-like species, limits its accessibility under physiological conditions.

■ ASSOCIATED CONTENT

Supporting Information

X-ray crystallographic data in CIF format, crystallographic data, computational data, and spectroscopic, reactivity, and biochemical studies on HS_2NO species. The Supporting Information is available free of charge on the ACS Publications website at DOI: 10.1021/acs.inorgchem.5b00831.

DOI: 10.1021/acs.inorgchem.5b00831
Inorg. Chem. XXXX, XXX, XXX–XXX

AUTHOR INFORMATION

Corresponding Authors

*E-mail: ivana.ivanovic-burmazovic@fau.de.
*E-mail: milos.filipovic@fau.de.

Author Contributions

The manuscript was written through contributions of all authors. All authors have given approval to the final version of the manuscript.

Notes

The authors declare no competing financial interest.

ACKNOWLEDGMENTS

We thank Dr. Carlos Dücker-Benfer for performing X-ray crystallography measurements of yellow crystals on a SuperNova dual diffractometer. This work was supported by the "Medicinal Redox Inorganic Chemistry" Emerging Field intramural grant from the Friedrich-Alexander University of Erlangen-Nuremberg.

DEDICATION

Dedicated to Prof. Rudi van Eldik on the occasion of his 70th birthday.

REFERENCES

(1) Palmer, R. M.; Ferrige, A. G.; Moncada, S. *Nature* **1987**, *327*, 524−526.
(2) Yang, G.; Wu, L.; Jiang, B.; Yang, W.; Qi, J.; Cao, K.; Meng, Q.; Mustafa, A. K.; Mu, W.; Zhang, S.; Snyder, S. H.; Wang, R. *Science* **2008**, *322*, 587−590.
(3) Garthwaite, J. *Eur. J. Neurosci.* **2008**, *27*, 2783−2802.
(4) Abe, K.; Kimura, H. *J. Neurosci.* **1996**, *16*, 1066−1071.
(5) Bogdan, C. *Nat. Immunol.* **2001**, *2*, 907−916.
(6) Whiteman, M.; Winyard, P. G. *Expert Rev. Clin. Pharmacol.* **2011**, *4*, 13−32.
(7) Whiteman, M.; Li, L.; Kostetski, I.; Chu, S. H.; Siau, J. L.; Bhatia, M.; Moore, P. K. *Biochem. Biophys. Res. Commun.* **2006**, *343*, 303−310.
(8) Li, L.; Rose, P.; Moore, P. K. *Annu. Rev. Pharmacol. Toxicol.* **2011**, *51*, 169−187.
(9) Yong, Q. C.; Cheong, J. L.; Hua, F.; Deng, L. W.; Khoo, Y. M.; Lee, H. S.; Perry, A.; Wood, M.; Whiteman, M.; Bian, J. S. *Antioxid. Redox Signal.* **2011**, *14*, 2081−2091.
(10) Yong, Q. C.; Hu, L. F.; Wang, S.; Huang, D.; Bian, J. S. *Cardiovasc. Res.* **2010**, *88*, 482−491.
(11) Eberhard, M.; Dux, M.; Namer, B.; Miljkovic, J.; Cordasic, N.; Will, C.; Fischer, M.; Suarez, S. A.; Bikel, D.; de la Roche, J.; Dorsch, K.; Kichko, T. I.; Leffler, A.; Babes, A.; Lampert, A.; Lennerz, J. K.; Jacobbi, J.; Marti, M. A.; Doctorovich, F.; Högestätt, E. D.; Zygmunt, P. M.; Ivanovic-Burmazovic, I.; Messlinger, K.; Reeh, P.; Filipovic, M. R. *Nat. Commun.* **2014**, *5*, 4381.
(12) Filipovic, M. R.; Milijkovic, J.; Allgaeuer, A.; Chaurio, R.; Shubina, T.; Herrmann, M.; Ivanovic-Burmazovic, I. *Biochem. J.* **2012**, *441*, 609−621.
(13) Cuevasanta, E.; Zeida, A.; Carballal, S.; Wedmann, R.; Morzan, U.; Trujillo, M.; Radi, R.; Estrin, D.; Filipovic, M. R.; Alvarez, B. *Free Radicals Biol. Med.* **2015**, *80*, 93−100.
(14) Miljkovic, J. L.; Kenkel, I.; Ivanovic-Burmazovic, I.; Filipovic, M. R. *Angew. Chem., Int. Ed.* **2013**, *52*, 12061−12064.
(15) Wedmann, R.; Bertlein, S.; Macinkovic, I.; Boeltz, S.; Miljkovic, J.; Munoz, L.; Herrmann, M.; Filipovic, M. R. *Nitric Oxide* **2014**, *41*, 85−96.
(16) Filipovic, M. R.; Miljkovic, J. L.; Nauser, T.; Royzen, M.; Klos, K.; Shubina, T.; Koppenol, W.; Lippard, S.; Ivanovic-Burmazovic, I. *J. Am. Chem. Soc.* **2012**, *134*, 12016−12027.
(17) Filipovic, M. R.; Eberhardt, M.; Prokopovic, V.; Mijuskovic, A.; Orescanin Dusic, O.; Reeh, P. W.; Ivanovic-Burmazovic, I. *J. Med. Chem.* **2013**, *56*, 1499−1508.
(18) Foster, M. W.; Hess, D. T.; Stamler, J. S. *Trends Mol. Med.* **2009**, *15*, 391−404.
(19) Hess, D. T.; Stamler, J. S. *J. Biol. Chem.* **2012**, *287*, 4411−4418.
(20) Broniowska, K. A.; Hogg, N. *Antioxid. Redox Signal.* **2012**, *17*, 969−980.
(21) Cortese-Krott, M. M.; Fernandez, B. O.; Santos, J. L.; Mergia, E.; Grman, M.; Nagy, P.; Kelm, M.; Butler, A.; Feelisch, M. *Redox Biol.* **2014**, *2*, 234−44.
(22) Berenyiova, A.; Grman, M.; Mijuskovic, A.; Stasko, A.; Misak, A.; Nagy, P.; Ondriasova, E.; Cacanyiova, S.; Brezova, V.; Feelisch, M.; Ondrias, K. *Nitric Oxide.* **2015**, *46*, 123−130.
(23) Cortese-Krott, M. M.; Fernandez, B. O.; Kelm, M.; Butler, A. R.; Feelisch, M. *Nitric Oxide.* **2015**, *46*, 14−24.
(24) Seel, F.; Kuhn, R.; Simon, G.; Wagner, M. *Z. Naturforsch. B* **1985**, *40b*, 1607−1617.
(25) Feher, F. Sulfur, Selenium, Tellurium. In *Handbook of Preparative Inorganic Chemistry*; Brauer, G., Ed.; Academic Press: New York, 1963; Vol. *1*, pp 346−353.
(26) Connelly, N. G.; T, D. P.; Green, M.; Kuc, T. A. *J. Chem. Soc., Dalton Trans.* **1977**, *1977*, 70−74.
(27) Martinsen, A.; Songstad, J. *Acta Chim. Scand. A* **1977**, *31*, 645−650.
(28) Rosenthal, J.; Lippard, S. *J. Am. Chem. Soc.* **2010**, *132*, 5536−5537.
(29) Sheldrick, G. M. *Acta Crystallogr., Sect. A* **2008**, *64*, 112−122.
(30) Dolomanov, O. V.; Bourhis, L. J.; Gildea, R. J.; Howard, J. A. K.; Puschmann, H. *J. Appl. Crystallogr.* **2009**, *42*, 339−341.
(31) Vanin, A. F.; Bevers, L. M.; Mikoyan, V. D.; Poltorakov, A. P.; Kubrina, L. N.; van Faassen, E. *Nitric Oxide* **2007**, *16*, 71−81.
(32) Vanin, A. F.; Poltorakov, A. P.; Mikoyan, V. D.; Kubrina, L. N.; van Faassen, E. *Nitric Oxide* **2006**, *15*, 295−311.
(33) Wang, X.; Kettenhofen, N. J.; Shiva, S.; Hogg, N.; Gladwin, M. T. *Free Radicals Biol. Med.* **2008**, *44*, 1362−1372.
(34) Zhang, D.; Macinkovic, I.; Devarie-Baez, N. O.; Pan, J.; Park, C.-M.; Carroll, K. S.; Filipovic, M. R.; Xian, M. *Angew. Chem., Int. Ed.* **2014**, *53*, 575−581.
(35) Grimme, S. J. *Comput. Chem.* **2003**, *24*, 1529−1537.
(36) Dunning, T. H., Jr. *J. Chem. Phys.* **1989**, *90*, 1007−1023.
(37) Kendall, R. A.; Dunning, T. H.; Harrison, R. J. *J. Chem. Phys.* **1992**, *96*, 6796−6806.
(38) Woon, D. E.; Dunning, T. H. *J. Chem. Phys.* **1994**, *100*, 2975−2988.
(39) Hättig, C.; Tew, D. P.; Köhn, A. *J. Chem. Phys.* **2010**, *132*, 231102.
(40) Peterson, K. A.; Adler, T. B.; Werner, H.-J. *J. Chem. Phys.* **2008**, *128*, 084102.
(41) Yousaf, K. E.; Peterson, K. A. *J. Chem. Phys.* **2008**, *129*, 184108.
(42) Yousaf, K. E.; Peterson, K. A. *Chem. Phys. Lett.* **2009**, *476*, 303−307.
(43) The ORCA program system: Neese, F. *WIREs Comput. Mol. Sci.* **2012**, *2*, 73−78.
(44) Furche, F.; Ahlrichs, R.; Hättig, C.; Klopper, W.; Sierka, M.; Weigend, F. *WIREs Comput. Mol. Sci.* **2014**, *4*, 91−100.
(45) Wilson, M. K.; Badger, R. M. *J. Chem. Phys.* **1949**, *17*, 1232.
(46) Liebeskind, S.; Korth, H. G.; de Groot, H.; Kirsch, M. *Org. Biomol. Chem.* **2008**, *6* (14), 2560−2573.
(47) Wang, K.; Hou, Y.; Zhang, W.; Ksebeti, M. B.; Xian, M.; Cheng, J.-P.; Wang, P. G. *Bioorg. Med. Chem. Lett.* **1999**, *9*, 2897−2902.
(48) Gritsan, N. P.; Pritchina, E. A.; Bally, T.; Makarov, A. Y.; Zibarev, A. V. *J. Phys. Chem. A* **2007**, *111*, 817−824.
(49) Bucci, M.; Papapetropoulos, A.; Vellecco, V.; Zhou, Z.; Pyriochou, A.; Roussos, C.; Roviezzo, F.; Brancaleone, V.; Cirino, G. *Arterioscler., Thromb., Vasc. Biol.* **2010**, *30*, 1998−2004.
(50) Kimura, H. *Antioxid. Redox Signal.* **2015**, *22*, 362−376.
(51) Timerghazin, Q. K.; Peslherbe, G. H.; English, A. M. *Phys. Chem. Chem. Phys.* **2008**, *10*, 1532−1539.
(52) Mikulski, C. M.; Russo, P. J.; Saran, M. S.; MacDiarmid, A. G.; Garito, A. F.; Heeger, A. J. *J. Am. Chem. Soc.* **1975**, *97*, 6358−6363.
(53) Steudel, R.; Eckert, B. *Top. Curr. Chem.* **2003**, *230*, 1−80.

DOI: 10.1021/acs.inorgchem.5b00831
Inorg. Chem. XXXX, XXX, XXX−XXX

(54) Tronc, M.; Huetz, A.; Landau, M.; Pichou, F.; Reinhardt, J. *J. Phys. B: Atom. Mol. Phys.* **1975**, *8*, 1160−1169.
(55) Bari, S. E.; Olabe, J. A.; Slep, L. D. *Adv. Inorg. Chem.* **2015**, *67*, 87−144.
(56) Southern, J. S.; Green, M. T.; Hillhouse, G. L.; Guzei, I. A.; Rheingold, A. L. *Inorg. Chem.* **2001**, *40*, 6039−6046.
(57) Serres, R. G.; Grapperhaus, C. A.; Bothe, E.; Bill, E.; Weyhermüller, T.; Neese, F.; Wieghardt, K. *J. Am. Chem. Soc.* **2004**, *126*, 5138−5153.
(58) Codesido, N. O.; Weyhermüller, T.; Olabe, J. A.; Slep, L. D. *Inorg. Chem.* **2014**, *53*, 981−997.
(59) Espey, M. G.; Miranda, K. M.; Thomas, D. D.; Wink, D. A. *Free Radicals Biol. Med.* **2002**, *33*, 827−834.
(60) Lin, R.; Farmer, P. J. *J. Am. Chem. Soc.* **2000**, *122*, 2393−2394.
(61) Sulc, F.; Immoos, C. E.; Pervitskiy, D.; Farmer, P. J. *J. Am. Chem. Soc.* **2004**, 1096−1101.
(62) Bartberger, M. D.; Fukuto, J. M.; Houk, K. N. *Proc. Natl. Acad. Sci. U. S. A.* **2001**, *98*, 2194−2198.
(63) Filipović, M. R.; Stanić, D.; Raicević, S.; Spasić, M.; Niketić, V. *Free Radical Res.* **2007**, *41*, 62−72.
(64) Ferrer-Sueta, G.; Radi, R. *ACS Chem. Biol.* **2009**, *4*, 161−177.
(65) Bartberger, M. D.; Liu, W.; Ford, E.; Miranda, K. M.; Switzer, C.; Fukuto, J. M.; Farmer, P. J.; Wink, D. A.; Houk, K. N. *Proc. Natl. Acad. Sci. U. S. A.* **2002**, *99*, 10958−10963.
(66) Hughes, M. N. *Biochim. Biophys. Acta* **1999**, *1411*, 263−272.
(67) Koppenol, W. H. *Inorg. Chem.* **2012**, *51*, 5637−5641.
(68) Galliker, B.; Kissner, R.; Nauser, T.; Koppenol, W. H. *Chemistry* **2009**, *15*, 6161−6168.
(69) Steudel, R. *Top. Curr. Chem.* **2003**, *230*, 153−166.
(70) Ivanova, L. V.; Anton, B. J.; Timerghazin, Q. K. *Phys. Chem. Chem. Phys.* **2014**, *16*, 8476−8486.

DOI: 10.1021/acs.inorgchem.5b00831
Inorg. Chem. XXXX, XXX, XXX−XXX